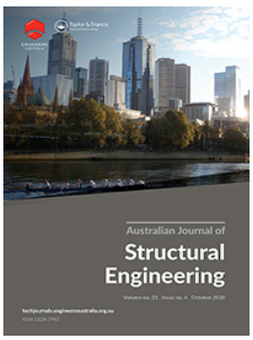

Taylor & Francis
Taylor & Francis Group

Australian Journal of Structural Engineering

ISSN: (Print) (Online) Journal homepage: https://engineersaustralia.tandfonline.com/loi/tsen20

Bending behaviour experiment of a prestressed concrete beam with metal bellows

Qingming Xiang , Xuansheng Cheng , Jiaxuan Su & Liang Ma

To cite this article: Qingming Xiang , Xuansheng Cheng , Jiaxuan Su & Liang Ma (2020) Bending behaviour experiment of a prestressed concrete beam with metal bellows, Australian Journal of Structural Engineering, 21:4, 279-293, DOI: 10.1080/13287982.2020.1796075

To link to this article: https://doi.org/10.1080/13287982.2020.1796075

Published online: 27 Jul 2020.

AUSTRALIAN JOURNAL OF STRUCTURAL ENGINEERING
2020, VOL. 21, NO. 4, 279–293
https://doi.org/10.1080/13287982.2020.1796075

Taylor & Francis
Taylor & Francis Group

ARTICLE

Bending behaviour experiment of a prestressed concrete beam with metal bellows

Qingming Xiang[a], Xuansheng Cheng[b,c], Jiaxuan Su[d] and Liang Ma[b]

[a]Wenzhou Traffic Quality Supervision Bureau, WenZhou, China; [b]Key Laboratory of Disaster Prevention and Mitigation in Civil Engineering of Gansu Province, Lanzhou University of Technology, Lanzhou, China; [c]Western Engineering Research Center of Disaster Mitigation in Civil Engineering of Ministry of Education, Lanzhou University of Technology, Lanzhou, ssssChina; [d]Wenzhou Traffic Engineering Test and Inspection Limited Company, WenZhou, China

ABSTRACT

In this paper, grouting compactness and load forms are taken as control conditions, and the bending behaviour of 8 PCBs (prestressed concrete beams) with metal bellows of different grouting compactness is experimentally examined. The strain and deflection of the prestressed beams are measured, and the failure process and failure modes are investigated under the action of different load forms. The rebar strain, bending bearing capacity and bending stiffness of the PCBs are explored, and a comparative analysis is conducted. The results show that the average strain is linearly distributed along the beam height for all PCBs. The load versus span deflection curve and rebar strain curve of the specimens show that the grouting compactness has little effect on the early stage of beam cracking, but the effect becomes increasingly obvious after the beam cracks. Under different load forms, when the grouting compactness of the PCB increases, the crack distribution becomes more concentrated, the spacing narrows, and the ductility decreases. The load-bearing capacity of the PCB with 100% grouting compactness can be improved by more than 30% compared with that of the prestressed beam with 0% grouting compactness of the metal bellows.

ARTICLE HISTORY
Received 20 November 2019
Accepted 10 July 2020

KEYWORDS
Prestressed concrete beam; grouting compactness; metal bellows; bending behaviour; experiment

1. Introduction

With the continuous development of bridge technology, prestressed concrete technology has been significantly improved. Because of unparalleled advantages, such as a light structure, strong spanning capacity, and delayed concrete cracking, prestress technology has been widely used in civil engineering (Du 1997; Zhao 2012). Prestressed concrete bridges have been constructed in China since the 1950s. Due to the experience amassed, China has constructed many prestressed concrete bridges with large spans. At the end of the twentieth century, China successfully built the Humen bridge, with a main span of 270 m, which indicates that China uses the most advanced prestressed concrete bridge technology worldwide (Ji and Fu 2010). However, with the massive construction of prestressed concrete bridges, problems gradually arise. In the actual production of prestressed beams, defects in the grouting quality of prestressed bellows are caused by human and technical factors. The presence of these voids weakens the bond strength between the prestressed reinforcement and the concrete; therefore, the prestressed tendon cannot be protected and is easily corroded, which will decrease the bearing capacity of the bridge and directly affect the safety of the structure within its service life.

Woodward studied 12 existing and 2 newly built bridges and found a lack of complete grouting in bridges in both age groups. Thus, sufficient pressure and continuity must be maintained to ensure full grouting of the pore canal (Woodward 1981). Based on the pore canal grouting of multiple existing bridges and a grouting test, Li and Yuan (Li and Yan 2010) made 5 posttensioned PCBs, and 4 beams were subjected to salt-accelerated corrosion for a period of 13 months (corrosion rate of 0.94 ~ 2.87%). Then, the 5 beams were subjected to a static load test at the one-third point. The flexural performance degradation characteristics due to corrosion of the prestressed steel strand in the concrete beams were studied. Oh and Kim (Oh and Kim 2004) studied the shear behaviour of posttensioned PCBs using experimental methods and found that the concept of average strain and principal strain could be used for a more accurate shear analysis in the study of posttensioned PCBs. Yao et al. (Yao, Jia, and Yu 2013) studied the influence laws of the shear span ratio, stirrup ratio, concrete strength and prestress degree on the failure mode and shear ductility via a shear behaviour test of 15 posttensioned prestressed ultrahigh-strength concrete beams with unbonded tendons. According to practical engineering projects, Jia and Meng (Jia and Meng 2015) experimentally studied the bending performance of the

CONTACT Xuansheng Cheng cxs702@126.com

prestressed superstrength concrete beam and analysed the effect of the depth and area of the prestressed tendon on the bending performance of the beam. They showed that the crack load, yield load, peak load and stiffness of the total test beams could be improved by reducing the depth of the prestressed tendon or increasing its area. In addition, the bending ductility of the beam could be improved by increasing the depth of the prestressed tendon or reducing its area. Meng et al. (Meng, Jia, and Wang 2013) performed mechanical tests on 4 PCBs with cohesive tendons and ultrahigh-strength concrete beams under vertical static loads and discussed the flexural performance of PCBs of superhigh strength. After analysing the experimental data of the stress process, failure shape, maximum crack width and midspan deflection, they showed that the flexural-failure-mode of the flexural-mode beams and the PCBs were basically identical when the crack width and deflection calculation formulas were revised based on the standards.

Because microcracks and micropores are inevitable in the fabrication of concrete materials, Xiong et al. (Xiong, Yu, and Zhang 2010) defined the negative damage variable based on the expression of the elastic modulus of concrete. The negative damage variable was introduced into the damage constitutive equation, and the mechanical behaviour of externally PCBs was analysed using the finite element method considering additional damage mechanics. Then, the change law of the elastic modulus of the PCB with the prestress was obtained. Zhou and Zhang (Zhou and Zhang 2015) conducted on-site static load tests of a bridge with the existing large-span concrete bridge load test method and established a three-dimensional finite element model of the bridge using ABAQUS to analyse the static load of the bridge via numerical simulation. Zhou et al. (Zhou, Pan, and Zhang 2013) performed a repeated low-cycle loading test on 9 posttensioned PCBs and 1 reinforced concrete beam. Then, they analysed the seismic performance, including the hysteretic performance, skeleton curve, displacement ductility, stiffness degradation and energy dissipation property, of the posttensioned prestressed beams. Cao et al. (Cao et al. 2014) conducted two static tests of posttensioning PCBs and a fatigue test in two stages to analyse the nonlinear dynamic characteristics of the beam damage level, and they found that the nonlinear dynamic characteristics could be used to detect the damage of PCBs. Limongelli et al. (JGJ55-2011 2011) studied the deterioration of the early warning signal of a PCB subjected to static and dynamic tests based on test data. By analysing the data from an accelerometer and a displacement sensor, they introduced the first modal frequency during damage under different test procedures and dynamic characteristics. Then, they determined the change in bending stiffness by monitoring during the dynamic testing and static testing processes. Minh et al. (Minh, Mutsuyoshi, and Niitani 2007) carried out a series of accelerated corrosion tests on prestressed concrete beams with metal sheaths under different grouting conditions by means of the electric accelerated corrosion method and tested the flexural behaviour of each prestressed concrete beam after corrosion. The relationship between the corrosion of the prestressed tendons and the bearing capacity of the beams was studied. The results showed that the corrosion of the sheaths and prestressed tendons decreased the bearing capacity of the prestressed concrete beams significantly, and the corrosion rate of the corrugated pipes and prestressed tendons was accelerated due to the insufficient grouting in the channel.

In summary, current studies mainly focus on researching new materials, new equipment and new technology, and the effect of the grouting compactness on a prestressed beam is not being considered. Therefore, in this paper, the effect of the grouting compactness on the structural safety and application of detection technology are the research topic. The cross-sectional strain, deflection, failure process and failure mode are analysed by experimentally studying the bending resistance of metal-bellow PCBs with different grouting compactness levels. The changes in the bearing capacity, ductility and flexural rigidity of the beams under different grouting compactness levels are discussed. The results provide a theoretical basis for the design and construction of posttensioned prestressed concrete structures.

2. Test technique

2.1. Specimen design and production

Posttensioned PCBs were made, and 4 metal-bellow PCBs with identical size and different grouting compactness levels were designed and manufactured; the parameters are shown in Table 1. The cross-sectional dimensions were 150 mm × 250 mm, and the span was 1800 mm. A vibrating rod was used to compact the moulding of 35 MPa self-mixing concrete in the prefabricated timber formwork; the concrete was then cured for 28 days. The longitudinal tensile main bar was a hot-rolled round steel bar with a diameter of 10 mm and a yield strength of 335 MPa. According to the structure requirements, the upper part of the beam included 2 hot-rolled round steel bars with a diameter of 10 mm and a yield strength of 335 MPa. The stirrup used a hot-rolled round steel bar with a diameter of 6 mm, a spacing of 100 mm, and a yield strength of 300 MPa. The prestressed steel wire with a diameter of 6 mm (1 × 7–6) and a tensile strength of 1270 MPa was used in a linear layout; the spacing from the prestressed steel wire to the bottom of the beam was 50 mm, and the concrete cover

Table 1. Numbers and parameters of the specimens.

Serial number	Specimen number	Width/mm	Height/mm	Compactness	*PPR*	Loading forms
1	PCB1-1	150	250	Full grouting porosity	0.34	Symmetrical loading loading
2	PCB1-2	150	250	2/3 grouting porosity	0.34	Symmetrical loading
3	PCB1-3	150	250	1/3 grouting porosity	0.34	Symmetrical loading
4	PCB1-4	150	250	Without grouting porosity	0.34	Symmetrical loading
5	PCB2-1	150	250	Full grouting porosity	0.34	Concentrated loading
6	PCB2-2	150	250	2/3 grouting porosity	0.34	Concentrated loading
7	PCB2-3	150	250	1/3 grouting porosity	0.34	Concentrated loading
8	PCB2-4	150	250	Without grouting porosity	0.34	Concentrated loading

*The prestressed concrete beams with 1/3 grouting (PCB1-2, PCB2-2) and 2/3grouting (PCB1-3, PCB2-3) can form 1/3 and 2/3 of the cross sections by using the self-weight of the grouting body to achieve the effect that the grouting is not full.

was 20 mm thick. Figure 1 shows the specimen sizes and reinforcement diagram. Figure 2 shows a photograph of a test beam.

In Table 1, *PPR* is the degree of prestressing. It is defined by the strength of the prestressed and common tendons in the component and represents the tension ratio that the prestressed tendon and common tendon bars bear in the ultimate state.

$$PPR = \frac{A_p f_{yp}}{A_p f_{yp} + A_s f_y}$$

where *PPR* is the degree of prestressing, A_p is the sectional area of the prestressed tendon,$f_{yp}$is the yield strength of the prestressed steel bar, A_s is the sectional area of the non-prestressed bar, andf_y is the yield strength of the common tendons.

2.2. Material properties

(1) Wire: the prestressed steel wire had a nominal diameter of 6 mm (1 × 7–6), a nominal area of 22 mm^2, a tensile strength of 1270 MPa, an elastic modulus of 2.05×10^5 MPa, and a tensile control stress of 889 MPa.

(2) Cement: ordinary Portland cement P.O42.5; the cement performance is shown in Table 2.

(3) Sand: sand in mud, containing less than 3% sand; the sieving curve of the sand is shown in Figure 3.

(4) Stone: 5–20 continuous graded gravel, containing less than 1% mud; the aggregate screening curve is shown in Figure 4.

(1) Reinforcement performance

The longitudinal steel bar used a hot-rolled ribbed steel bar with a diameter of 10 mm and a yield strength of 335 MPa; the stirrup used a hot-rolled round steel bar with a diameter of 6 mm, a spacing of 100 mm, and a yield strength of 300 MPa. To obtain the yield strength, ultimate strength, and extensibility of the steel bars, two steel bars with different specifications were reserved from the same batch. The elasticity

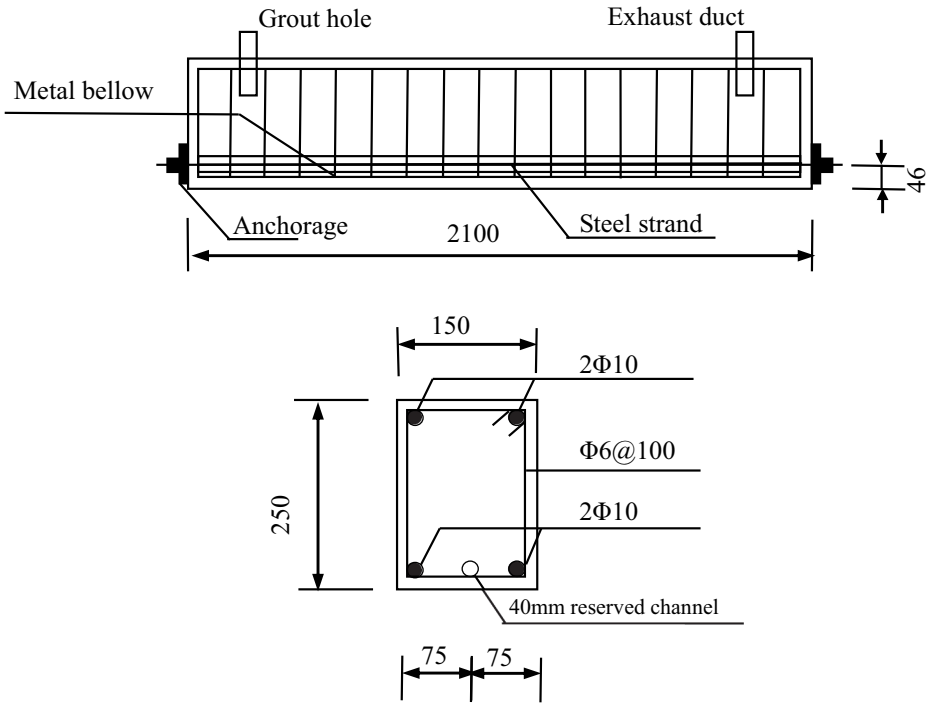

Figure 1. Dimensions and reinforcement diagram of the test beams.

Figure 2. Photo of test beams.

Table 2. Cement property.

Cement fineness /(m^2/kg)	Time of setting /min		Compression strength /MPa		Rupture strength /MPa	
	Initial set	Final set	3d	28d	3d	28d
350	173	238	27.3	51.6	6.0	7.4

modulus was obtained according to the code for the design of concrete structures of China. The material properties of the steel bars are shown in Table 3.

(6) Strength of concrete

The PCBs used poured C35 concrete, and all specimens were cast in the same period. Simultaneously, 6 cubic specimens (150 mm × 150 mm × 150 mm) of concrete were reserved to measure their compressive strength. The specimens were made using a plastic mould; the outdoor and test specimens were simultaneously cured for 28 days to ensure that the concrete properties could be tested. According to the relationship between the elastic modulus and the compressive strength obtained by the China Construction Science Research Institute after many experimental measurements and statistical analysis, the elastic modulus can be expressed as

$$E = \frac{10^5}{2.2 + \frac{34.7}{f_{cu,k}}}$$

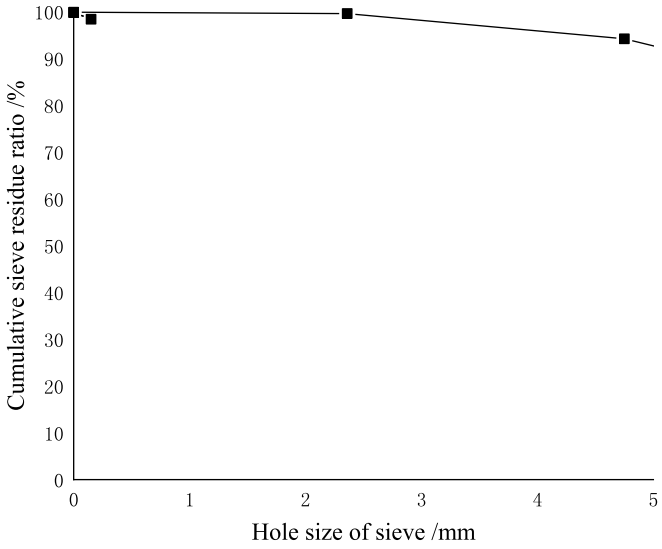

Figure 3. The sieving curve of the sand.

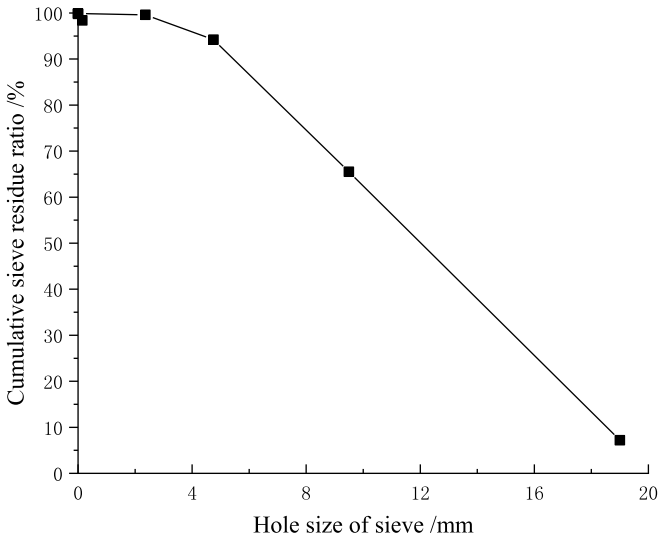

Figure 4. The aggregate screening curve.

Table 3. Mechanical property of the rebar.

Reinforcement category	Diameter /mm	Steel area /mm^2	Yield strength /MPa	Ultimate strength /MPa	Extensibility /%	Modulus of elasticity /×10^5 MPa
Common reinforcement	10	78.1	352.5	474.9	18.3	2.10
Stirrup	6	27.9	314.7	434.2	21.6	2.10

The measured mechanical properties are shown in Table 4. By substituting the compressive strength $f_{cu,k} = 37.7MPa$ of the cubic specimens obtained from the experiment into the equation, we have obtained that the elastic modulus of concrete: $E = 3.21 \times 10^4\ MPa$.

2.3. Concrete mix ratio

In this paper, the concrete mix ratio was designed according to the *Common concrete mix design* (Limongelli, Siegert, and Merliot et al. 2016); the mixture ratio is shown in Table 5.

2.4. Bellow parameters

At present, as prestressed concrete structures are used more and more widely in buildings, post-tensioned prestressed concrete structures are also used more and more. Bellows are mainly used to form holes in components of post-tensioned prestressed concrete structures. The usage is to form a reserved hole in the concrete so that prestressed steel pipes can pass through. It is widely used in projects such as high-rise buildings and bridges. Due to its good sealing performance and no water seepage, it can prevent the pollution of harmful substances penetrating through pipelines and ensure the durability of the structure. The bellows of the posttensioned prestressed concrete test beams are made of metal (Mu 2017), and the parameters of these materials are shown in Table 6.

2.5. Grouting compactness control

According to this standard, the duct grouting compactness of prestressed concrete beams is divided into four situations, namely, full grouting porosity, 2/3 grouting porosity, 1/3 grouting porosity, without grouting porosity. The control of duct grouting compactness of post-tensioned concrete beams is realised through controlling the volume of mortar pressed into duct. For prestressed concrete beams with grouting compactness of 1/3 (PCB1-2, PCB2-2) and 2/3 (PCB1-3, PCB2-3), the 1/3 and 2/3 of the section are formed by the self-weight of the pressed mortar to achieve the effect of grouting compactness. After grouting is completed, ultrasonic non-destructive testing is carried out on 8 test beams (full grouting porosity, 2/3 grouting porosity, 1/3 grouting porosity, without grouting porosity) to detect whether the compactness of duct grouting is accurate and ensure the smooth progress of subsequent tests.

Table 4. Compressive strength of the concrete.

Specimen number	Concrete strength/MPa	Mean intensity/MPa	Modulus of elasticity/ ×10^4 MPa
C1-1	37.5	37.7	3.21
C1-2	36.8		
C1-3	39.1		
C1-4	37.4		
C1-5	37.0		
C1-6	38.3		

Table 6. Bellows material parameters.

Bellows material	Diameter/ mm	Wall thickness/mm	Yield strength/ MPa	Modulus elasticity/MPa
Metal	40	0.3	235	2.05×10^5
Plastics	40	3	40	2×10^5

2.6. Loading device and layout of the measuring points

A portal-type vertical loading device was used in the test; this device used loading equipment such as a distributing beam and a jack, which are shown in Figure 5. In the test, a positive loading was used with two loading modes: symmetrical loading and concentrated loading with manual grading loading (implementation of hierarchical loading by manually controlled loader). The calculated load value was 50 kN, and each load stage was 10% of the load value. To obtain more accurately measure the crack load values of the structure, the calculated cracking load reached 90%, and each stage of the loading proceeded according to the load value of 5%.

When the specimen was cracked, loading continued at 10% of the predicted ultimate load before the non-prestressed steel bars yielded. At the yield load, the loading style was adjusted to displacement control. To prevent the sudden fracture of the test beam, which

Table 5. Concrete mixture ratio.

Water cement ratio W/C	Sand coarse aggregate ratio /%	Water /(kg/m^3)	Cement /(kg/m^3)	Sand /(kg/m^3)	Cobblestone /(kg/m^3)
0.41	39	168	409	713	1115

Figure 5. Test setup.

would damage the measuring instrument, the increment of displacement per stage was set to 2 mm until the specimen could not continue to bear the damage. The loads were measured using load sensors (Wang 2013).

Each load stage was applied for 10 min. Then, the test phenomena were recorded; the crack width was measured, and the crack development was observed.

Figure 6 shows the layout of the measuring points. On each side of the prestressed beam, at the section of the middle span, the section of the 1/4 span and the section of the 1/8 span, with 3 concrete strain plates were arranged along the beam height to test the distribution of the cross-sectional strain in the concrete along the beam height. A WY-50 displacement sensor was used to test the beam deflection; the measuring range was 50 mm, and the sensitivity was 200 με/mm. The sensors were installed at the 1/2 section, 1/4 section, and 1/8 section of the test beam to test the beam deflection. The load sensor of the hydraulic pump and jack loading system for obtaining the distribution of the vertical load on the beam was directly installed under the jack (20 t). The load strain, displacement load, etc. were collected through the DH3816 acquisition system.

2.7. The loading system

Preloading is required before a test beam is loaded. The preloading is generally carried out 2–3 times, proceeded by 3 stages. The preloading value is usually 10% of the estimated ultimate load value and less than 70% of the estimated cracking load value.

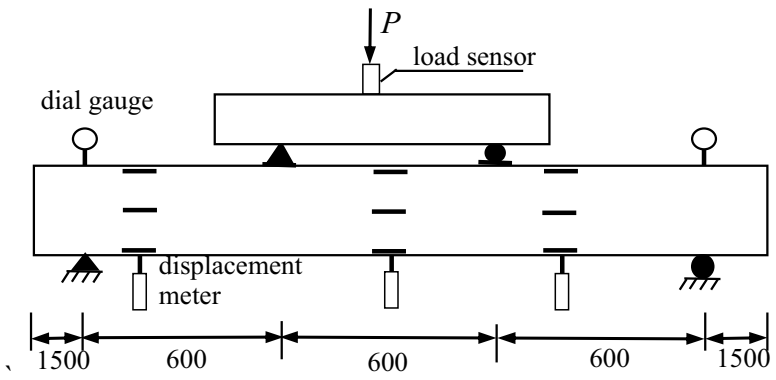

Figure 6. Layout of the measuring points/mm.

The loading of prestressed concrete beam in this study was a grading loading, and the load added to each stage is 10% of the estimated ultimate load. Because the experiment was designed to study the crack resistance of the prestressed concrete beams, in order to obtain the measured value of the cracking load of the prestressed concrete beam more accurately, when the loading reached 90% of the estimated cracking load value, the additional loading of each stage was 5% of the estimated cracking load value. After the test beam cracked, the loading value of each stage continued to increase by 10% of the estimated ultimate load value before the non-prestressed bar yielded. After the yield load was reached, the loading system was adjusted to displacement control loading. To prevent sudden breakage of the test beam, which damages the measuring instrument, the displacement increment was controlled to 2 mm until beam failure could not continue. After the loading of each stage was applied and held for approximately 10 min, the failure mode and crack development of the test beam were observed, and the relevant records were obtained.

3. Test results

3.1. Failure process and destruction forms

The PCBs of different grouting compactness levels under different load forms should be preloaded to check the instruments and data acquisition system and ensure proper operation before loading begins. At the beginning of loading, when the applied load was small, the deflection and concrete strain were small. In the early stage of loading, the deflection and concrete strain increased with the load, and the trend of variation was linear and monotonic. When the load increased to the cracking load, the first vertical crack appeared in the middle of the lower edge of each test beam, and the prestressed beam began to crack (fracture stage). With increasing load, the crack width of the pure bending section component increased, and the crack gradually extended upward; moreover, new, small cracks were observed. Gradually, the reinforced concrete tensile part of the beam failed, the neutral axis constantly moved, and diagonal cracks appeared at the loading point immediately below the vertical cracks between the loading points. With increasing load, the impacts of the loading points extended; both deflection and crack width clearly increased at an increasing rate, the increase in strain of the steel bar increased and destroyed the bonds in the concrete near the crack, and the fractures widened and extended upward. When the load continued to increase, the stress of the bar remained unchanged, whereas the strain increased until the prestressed beams of the pure bending section crushed near the upper loading point of the concrete. At this stage, a crisp crackling sound was heard, the beam bearing capacity sharply decreased, and the load was stopped. The fracture development in each beam after failure is shown in Figure 7.

According to the experimental observation and analysis, under the action of symmetrical loading and concentrated loading, the failure of a test beam is caused by the crushing of the concrete in the compression zone after tensile yielding. At an identical grouting compactness, the bearing capacity of the beam under symmetrical loading is higher than that of the prestressed beam under concentrated loading, which shows that the effect of the concentrated loading is more detrimental to the prestressed beam than the effect of the symmetrical loading. The bearing capacity of the prestressed beam increases with the grouting compactness, the fracture distribution increases with the grouting compactness, and the fracture spacing narrows. This phenomenon may be because the prestressed tendons and surrounding concrete are between the tight gripping force of the PCBs without grouting porosity, making the middle of the prestressed tendons more fully exhibit a tensile effect. Thus, the bearing capacity of the prestressed beam with low compactness distributes evenly along the entire prestressed tendon. The entire prestressed tendon can be controlled by the strain; the strain is relatively uniform, but the plastic hinge area may be more stable and able to bear the load.

3.2. Test results

Under symmetrical loading and concentrated loading, the measured cracking load, cracking deflection, ultimate load and maximum deflection of each test beam are shown in Table 8.

Table 7 shows that the posttensioned PCB crack deflection, crack load, ultimate load and maximum deflection increase with the grouting compactness. The main reason for this behaviour is that when the PCB has 100% grouting compactness under a load, the entire beam should be prestrained, and the surrounding concrete tendons should be consistent. Therefore, there is a strong bond between the prestressed reinforcement and the surrounding concrete, enabling the full cross section of the prestressed reinforcement to engage. The bearing capacity of the PCB beam is more than 30% higher than that of the prestressed beam with 0% grouting compactness, which highlights the importance of the grouting quality on the load-bearing capacity of the prestressed structure.

4. Comparison and analysis of results

4.1. Strain analysis of concrete

According to the test results for the concrete beams under strain, the curves along the height of the 8 test

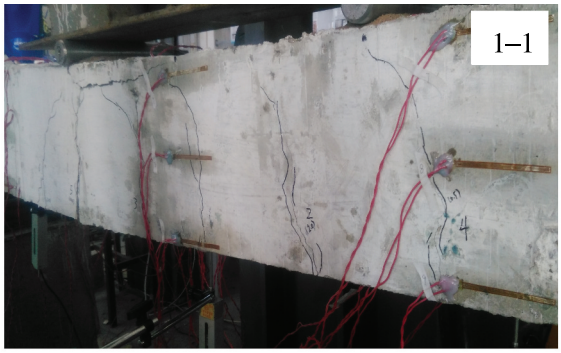

(a) PCB1-1

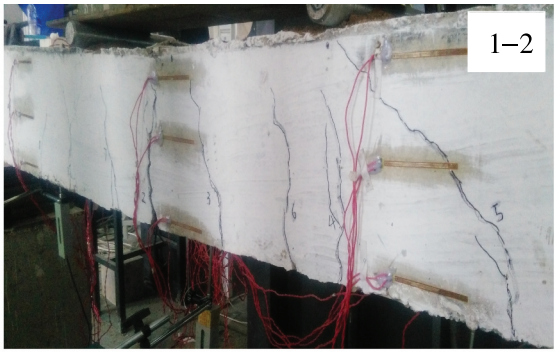

(b) PCB1-2

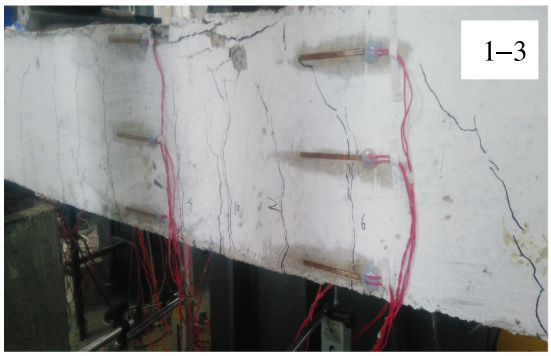

(c) PCB1-3

(d) PCB1-4

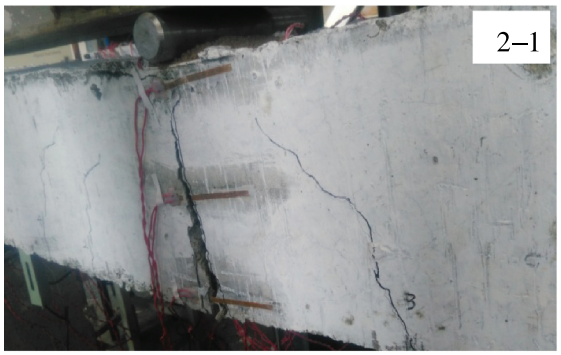

(e) PCB2-1

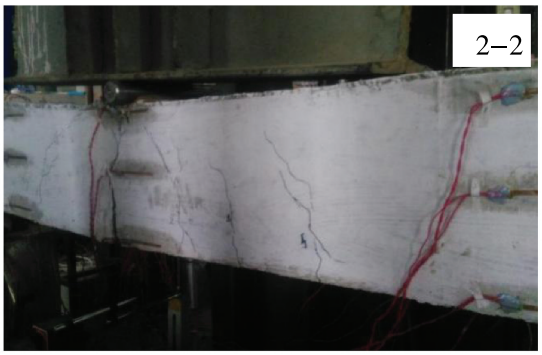

(f) PCB2-2

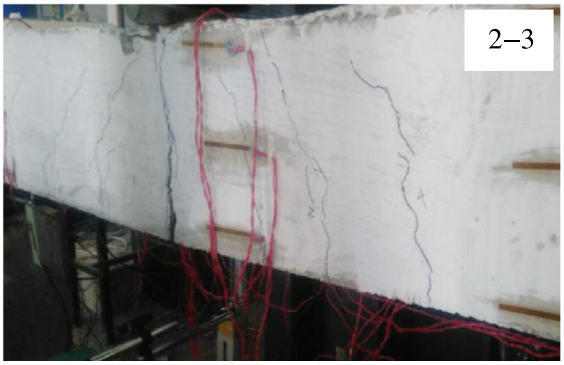

(g) PCB2-3

(h) PCB2-4

Figure 7. Failure patterns of the specimens.

Table 7. Grading standard for duct grouting compactness.

Evaluation grade	Description of grouting state
Grade A	Duct grouting is full, or there are small honeycomb bubbles on the upper part of corrugated pipe, which are not in contact with prestressed tendons.
Grade B	There is a gap in the upper part of the corrugated pipe, which is not in contact with the prestressed reinforcement.
Grade C	There is a gap in the upper part of the corrugated pipe, which is in contact with the prestressed reinforcement.
Grade D	There is no mortar on the upper part of corrugated pipe, which is in contact with prestressed reinforcement and is seriously short of mortar. Grade D can be divided into grades D_1, D_2 and D_3.

Table 8. Test results of the beams.

Specimen number	Grouting compactness	Cracking load P_{cr}/kN	Ultimate load P_u/kN	f_{cr}/mm	f_u/mm	p_{cr}/p_u
PCB1-1	Full grouting porosity	31.6	79.1	1.61	20.38	0.40
PCB1-2	2/3 grouting porosity	36.8	86.8	1.92	22.03	0.42
PCB1-3	1/3 grouting porosity	42.5	93.2	2.15	24.46	0.46
PCB1-4	Without grouting porosity	45.3	103.7	2.35	27.20	0.44
PCB2-1	Full grouting porosity	23.4	54.6	1.45	21.46	0.43
PCB2-2	2/3 grouting porosity	26.7	61.3	1.5	23.39	0.44
PCB2-3	1/3 grouting porosity	31.2	70.1	1.96	24.32	0.45
PCB2-4	Without grouting porosity	35.5	73.7	2.43	27.49	0.48

beam at each load level can be obtained, as shown in Figure 8. Thus, the effects of different load grades on the change in cross-sectional strain along the beam height can be analysed.

As shown in Figure 8, under the action of symmetrical loading and concentrated loading, the cross-sectional strain distribution along the height of the PCB with metal bellows and different grouting compactness values is approximately linear. Thus, the beam can satisfy the plane section assumption and is not affected by the grouting compactness or load forms. From the concrete strain curve of the mid-span section of the concrete beam, it can be seen that before the prestressed concrete beam cracks, each beam is in a linear elastic working state, and the ratio between the height of the compression zone of the mid-span section to the effective height of the section is approximately between 0.4 and 0.5. With the increasing load, when the non-prestressed tendons begin to yield, the ratio between the height of the compression zone of the mid-span section to the effective height of the section changes in the range of approximately between 0.3 and 0.4; when the concrete at the upper edge of the beam is crushed and cracked, the ratio between the height of the compression zone of the mid-span section to the effective height of the section changes in the range of approximately between 0.2 and 0.3. However, after cracking of the beam, the height of the compression zone of the beam increases with the increase of grouting compactness under the action of approximately similar load level. Which indicates that when other conditions are the same, the duct grouting compactness has little effect on the height of the section compression zone before cracking of prestressed concrete beams, but it has more obvious effect on the height of the section compression zone after cracking of prestressed concrete beams. It can be seen that improving the duct grouting compactness can make full use of the characteristics of strong compressive capacity of concrete and improve the bending bearing capacity of beams.

4.2. Strain analysis of steel bars

To study the change rule of the strain of tension reinforcement in prestressed beams with metal bellows under different grouting porosities, gauges were attached to the longitudinal reinforcement bars in the midspan of the prestressed beam to measure the strain of the reinforcement. The load-rebar strain curves of the prestressed beams with metal bellows at different grouting compactness levels were compared, as shown in Figure 9.

As shown in Figure 9, under identical load forms and load grades, at the maximum tensile strain of the longitudinal steel bar, a lower grouting compactness corresponds to a greater tensile strain of the reinforced concrete beam. Under different load forms, the strain difference was not obvious for prestressed beams with different grouting compactness levels before concrete cracking. But the strain difference of prestressed beams with different grouting compactness became increasingly obvious after cracking, because of the higher grouting compactness, the bond strength between the prestressed reinforcement and the surrounding concrete of the PCB was strong, the resistance force caused by the deformation was strong during early cracking, the strain of the non-prestressed tendon was relatively small, the bond strength between the tendon and the concrete decreased when the beam cracked, and the strain of the non-prestressed tendon more rapidly increased. When the beam cracked, the bond strength between the prestressed tendon and the surrounding concrete rapidly decreased for the prestressed beam

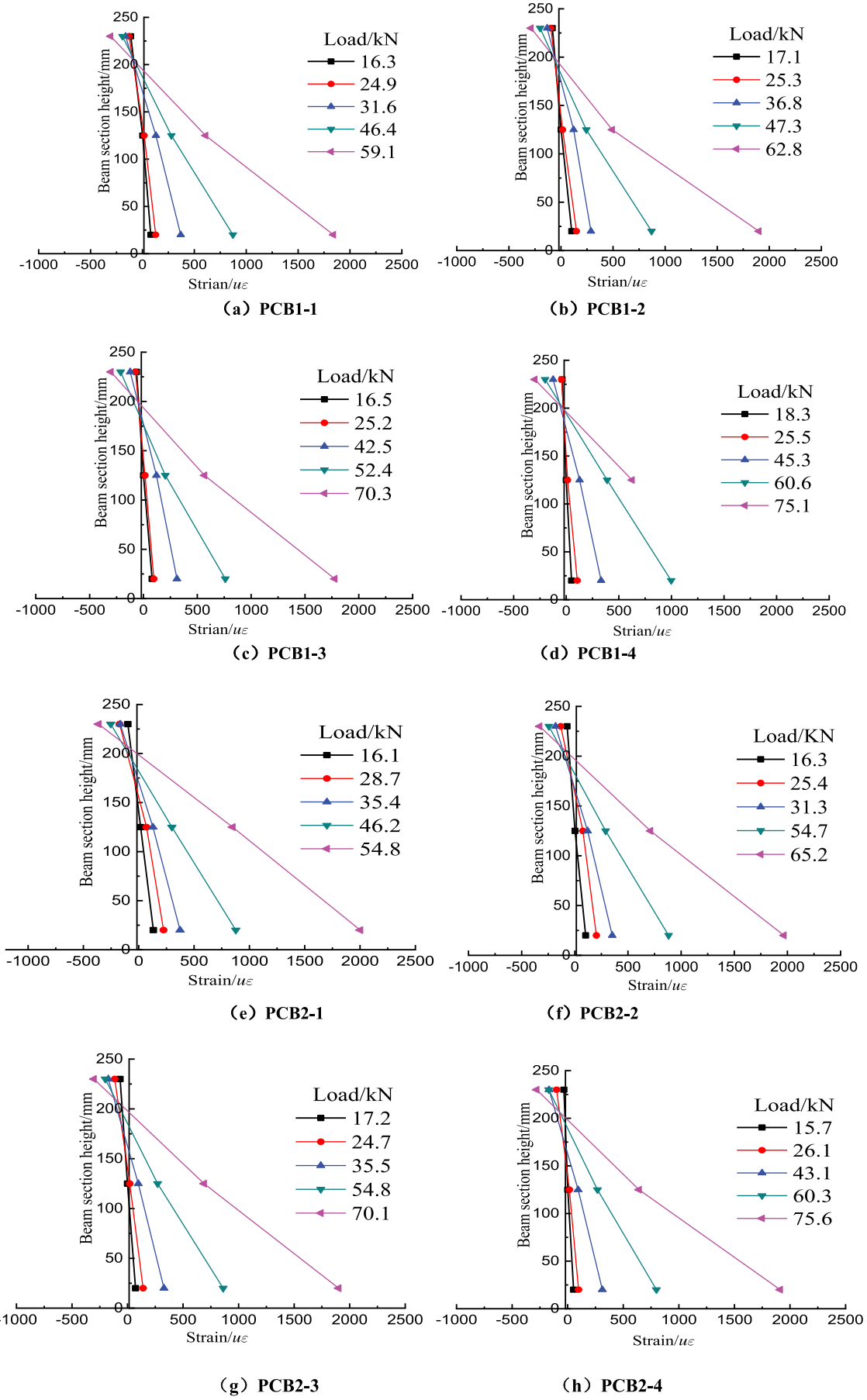

Figure 8. Strain at the midspan sections of the beam.

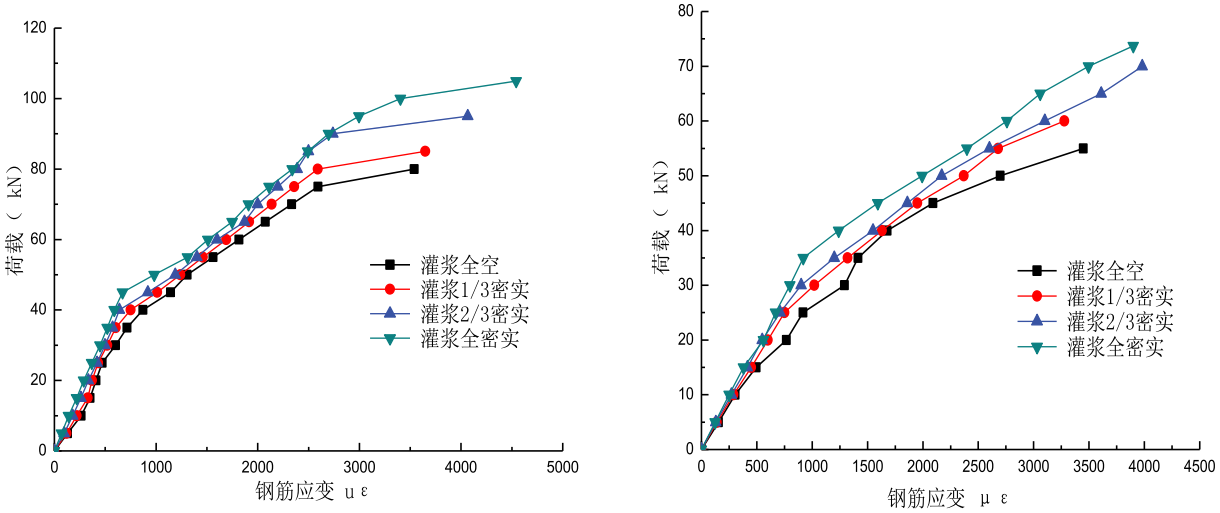

(a) Symmetrical loading **(b) Concentrated loading**

Figure 9. Tension bar load versus strain curves of the beams.

with full grouting porosity, and the strain of the non-prestressed tendon increased more rapidly than that of the prestressed beam with lower grouting compactness.

4.3. Load-deflection curve and bearing capacity

According to the measured span displacements of the metal-bellow PCBs, the load versus deflection curves of the metal-bellow PCBs with different grouting compactness levels under different load forms were obtained through displacement correction, as shown in Figure 10. The effects of the grouting compactness and load forms on the deflection of the PCBs were compared and analysed.

As shown in Figure 10, the beam load-deflection curve can be roughly divided into three sections: 1) For the load value of 40–48% p_u (p_u is the ultimate load), before the beam entered the elastic stage, the PCB versus deflection curves for different grouting compactness values had basically identical trends. Specifically, the slopes of the curve exhibited little difference; for small deformation, the deflection difference was not obvious and linearly changed with increasing load. 2) When the load increased, the concrete began to crack, and the test beam deflection growth rate significantly increased compared to that before cracking initiated. 3) The curve became increasingly flat. The graph shows that the grouting compactness test beams had different deflection growth rates during loading; when the load gradually increased, a lower grouting porosity corresponded to a greater slope of the curve and a lower growth rate. When reaching the same load stage (such as critical state of cracking and ultimate bearing state),

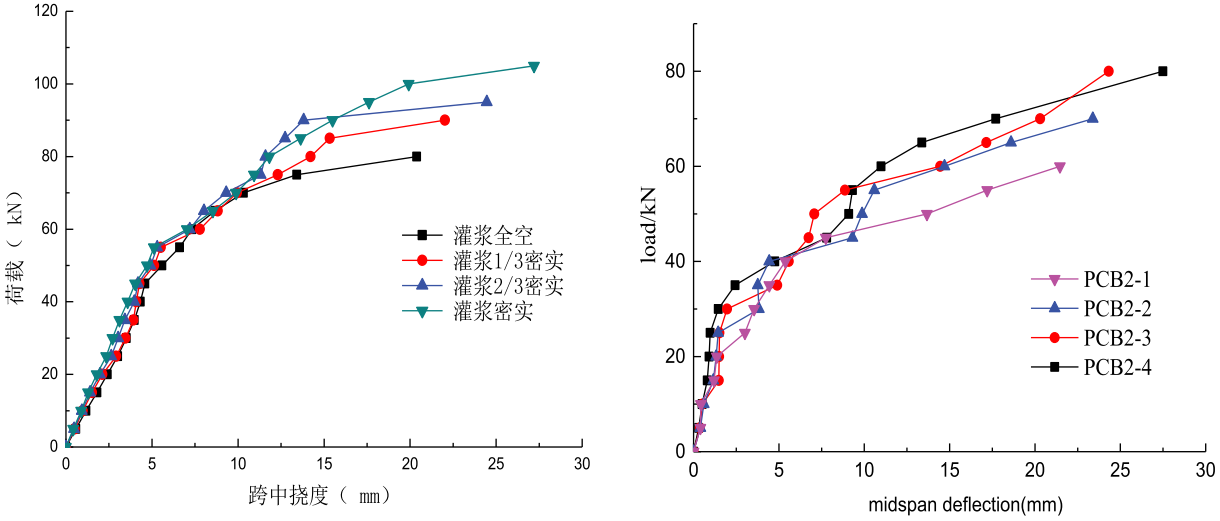

(a) Symmetrical loading **(b) Concentrated loading**

Figure 10. Load versus deflection curves of the beams.

considering the measurement error of individual data, the midspan deflection of the low-grouting-porosity beam was smaller than those of other prestressed beams with higher grouting compactness levels. For prestressed concrete beams with different loading methods, when the grouting compactness is the same, the deflection of printed circuit board under concentrated load is smaller than that under symmetrical load under the same load level.

4.4. Ductility analysis

The monotonic loading form was used in this paper. Under different loading forms, the load-displacement curve can replace the skeleton curve for analysis of the displacement ductility of prestressed beams with grouting compactness (Wang and Han 2008). Because scholars at home and abroad have different views on the ductility of the components, the definitions of ductility vary. The commonly accepted definitions of ductility are described by using the following data: the hysteretic curve, energy dissipation capacity, rotation capability of plastic hinge, displacement ductility coefficient of the structure or component, section curvature, ductility coefficient, etc. However, for static analysis, the ductility index includes the curvature ductility and displacement ductility coefficient. Therefore, in this paper, the displacement ductility coefficient was used to define the ductility of prestressed beams with grouting compactness; the displacement ductility coefficient is the ratio of the yield displacement and ultimate displacement of the component (Zhang, Zhang, and Yang 2017). The initial yield displacement Δy was taken as the deflection when the steel bar in the tensile region yielded. The specific value was determined by the measured load-deflection curves and strain value of the steel bar. The limit displacement Δu was taken as the displacement that corresponded to the ultimate load when the bearing capacity decreased to 85%. The displacement ductility coefficient μ can be calculated as follows:

$$\mu = \frac{\Delta u}{\Delta y}$$

Table 9 shows the displacement ductility coefficients of the PCBs with metal bellows at different grouting compactness levels.

Table 9 and Figure 11 show that under the action of the two loading forms, all the ductility coefficients of the PCBs with different grouting compactness levels are approximately 3.0; the ductility is good. The ductility coefficient of the metal-bellow PCB decreases with the increase in grouting compactness, i.e., the prestressed concrete structures with low grouting compactness have better ductility than the prestressed concrete structures with higher grouting compactness. For a PCB with higher grouting compactness, the prestressed reinforcement and bond of the tendon to the surrounding concrete cross section with high stress produce more concentrated cracks in the beam. When the load increases, the crack stress gradually increases, making the midspan prestressed reinforcement more likely to yield, and the yield occurs soon after the limit state is reached. However, for

Table 9. Ductility coefficients of displacement.

Specimen number	Grouting compactness	Δy/ mm	Δu/ mm	μ
PCB1-1	Full grouting porosity	8.89	28.33	3.19
PCB1-2	2/3 grouting porosity	10.02	28.69	2.86
PCB1-3	1/3 grouting porosity	11.34	30.96	2.73
PCB1-4	Without grouting porosity	12.70	33.21	2.61
PCB2-1	Full grouting porosity	7.16	26.49	3.70
PCB2-2	2/3 grouting porosity	8.30	28.39	3.42
PCB2-3	1/3 grouting porosity	9.12	29.28	3.21
PCB2-4	Without grouting porosity	10.98	34.70	3.16

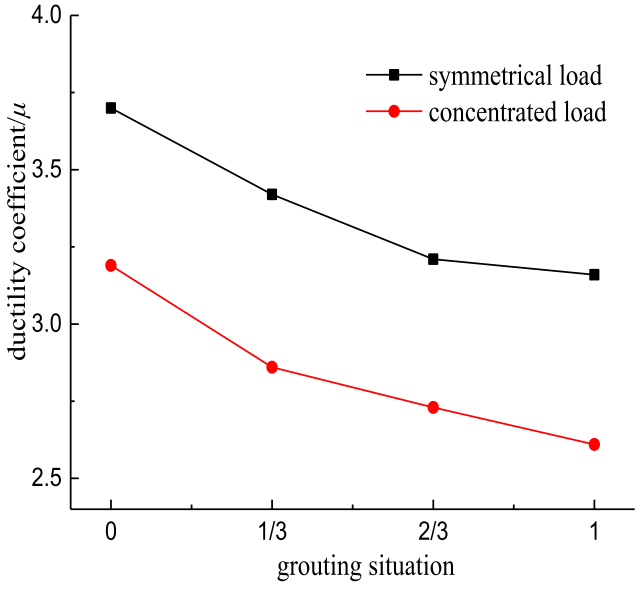

Figure 11. Comparison of the ductility coefficients.

a prestressed beam with lower grouting compactness, the prestressed tendon distribution along the span of the beam is more uniform. There is no stress concentration in the span of the beam, the prestressed tendon does not easily yield, and the ductility is relatively high.

The displacement ductility coefficient in the midspan of the PCB with metal bellows under the action of a concentrated loading is 17.4% lower than that of the PCB with metal bellows under the symmetrical loading of two points.

4.5. Stiffness analysis

Focusing on the concentrated loading and symmetrical loading to analyse the effect of the grouting compactness of metal bellows on the short-term stiffness of a prestressed beam, we consider two prestressed beams with different grouting compactness levels. These beams undergo identical load levels before and after cracking to determine the effect of the grouting compactness on the beam deflection curve, as shown in Figures 10 and 11.

As shown in Figures 12 and 13, the grouting compactness is one of the factors that affect the short-term stiffness of a prestressed beam. Under an identical load form, a lower grouting compactness corresponds to a larger deflection of the beam and a lower short-term stiffness. Before cracking, the effect of grouting compactness on the stiffness of the beam is relatively small, and the curve is slowly changing. After cracking, the curve becomes steeper with a decrease in grouting compactness, and the effect of the grouting compactness on the stiffness is more obvious. Thus, in an actual bridge, a high grouting compactness results in a higher safety factor after use. When the grouting compactness is low, the stiffness will rapidly weaken, and the security reserve will be low.

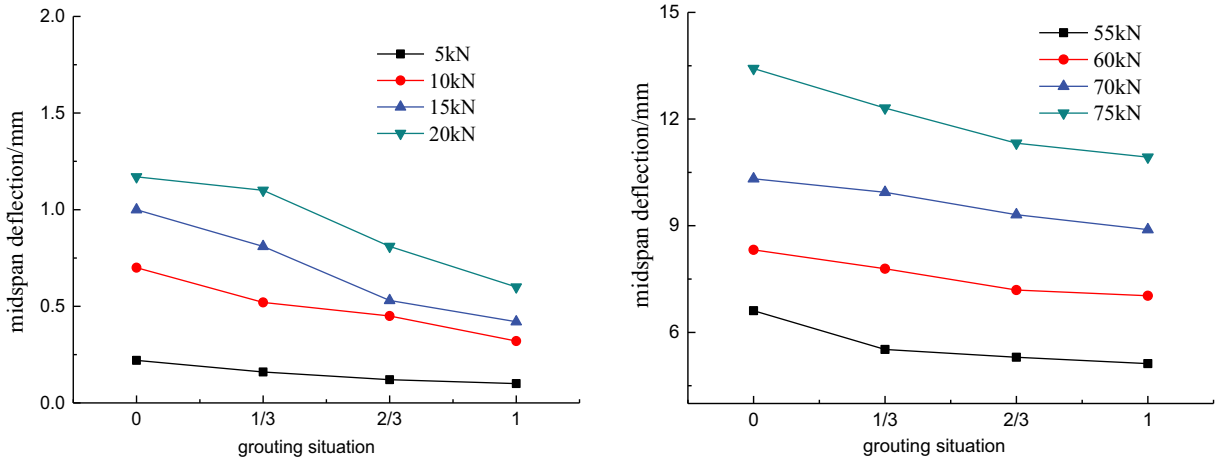

(*a*) Before cracking (*b*) After cracking

Figure 12. Deflection curve before and after cracking of the prestressed beams under symmetrical loading.

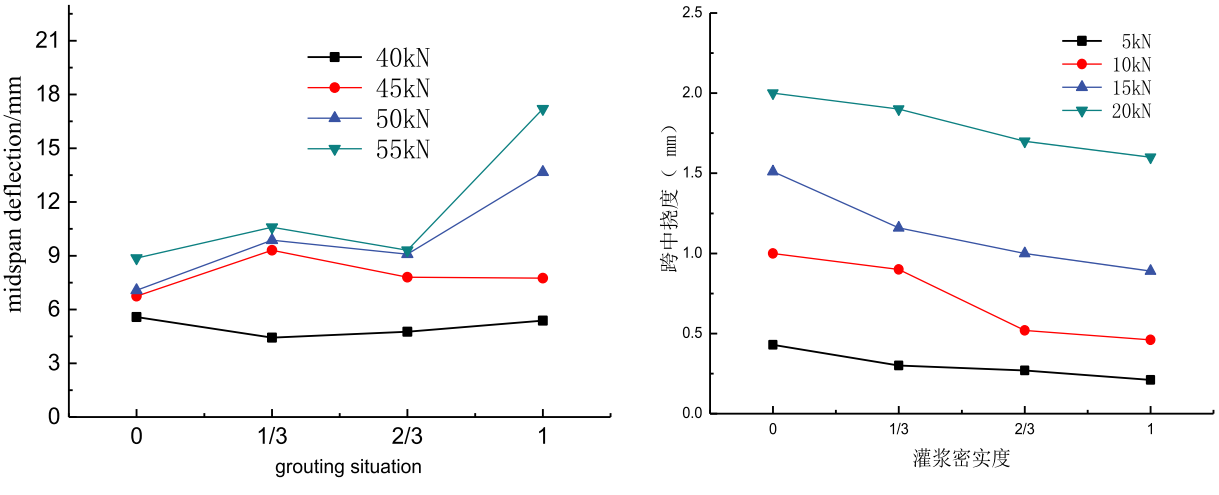

(b) After cracking (a) Before cracking

Figure 13. Deflection curve before and after cracking of prestressed beams under concentrated loading.

5. Conclusions

(1) The bearing capacity of a PCB with metal bellows and 0% grouting compactness can be improved by more than 30% compared with those of prestressed beams with metal corrugated bellows and 100% grouting compactness. The bearing capacity of a beam under a symmetrical loading is greater than that under a concentrated loading, which can be increased by 30–45%, indicating that a sudden concentrated loading should be avoided in existing prestressed structures.

(2) For lower grouting compactness, because of the force between the tendons and the surrounding concrete, the stress of the prestressed tendon is greater at the midspan section, the cracks are more concentrated, and the spacing is smaller. For a prestressed beam with higher grouting compactness, the tendon stress along the cross beam distribution is more uniform, the beam span is not under high stress, and the prestressed reinforcement does not easily yield. Thus, the ductility of the prestressed concrete structure with low grouting compactness is superior to the prestressed concrete structure with high grouting compactness. Specifically, the ductility increases with decreasing grouting compactness.

(3) When the load is within a certain range, the plane section assumption remains applicable to the flexural performance of PCBs with grouting compactness. The bar strain-deflection curve of prestressed beams with metal corrugated bellows can be roughly divided into three sections. When the load value is 40–48% p_u (p_u is the ultimate load), the beam is in the elastic stage. In addition, the grouting compactness has little effect, as the overall trends of the curves for beams with different grouting compactness levels are basically identical, and the effect of the concrete cracking is obvious.

(4) With the increase in grouting compactness, the short-term stiffness increases; the effect of the grouting compactness is not obvious before concrete cracking. However, the effect of the grouting compactness on the prestressed beam stiffness in PCBs mainly occurs after cracking. Therefore, in an actual bridge, a higher grouting compactness corresponds to a higher safety factor for the later stages of the beam; at a lower grouting porosity, the stiffness weakens more rapidly in the later stage, and the safety factor is lower.

Disclosure statement

The authors declare that there are no conflicts of interest regarding the publication of this paper.

Funding

This paper is a part of science and technology project in the Zhejiang Traffic Quality Supervision Bureau [Grant number: ZJ201602], and a part of the National Natural Science Foundation of China [Grant number: 51968045], and a part of science and technology project in China Railway 21th Bureau Group [Grant number: 14B-3].

References

Cao, H., X. Zheng, J. M. Hua, and Z. M. Hu. 2014. "Damage Detection of Prestressed Concrete Beams Based on Nonlinear Dynamic Characteristics." *Engineering Mechanics*. 31(2):190–194.

Du, G. C. 1997. "Applicationg and Development of Prestressed Concrete for Buildings in the past 40 Years." *China Civil Engineering Journal*. 30(1):3–15.

JGJ55-2011. 2011. *Specification for Mix Proportion Design of Ordinary Concrete*. Beijing: China Building Industry Press.

Ji, B. H., and Z. Q. Fu. 2010. "Analysis of Chinese Bridge Collapse Accident Cause in Causes in Recent Years." *China Civil Engineering Journal*. 43(S1):495–498.

Jia, J., and G. Meng. 2015. "Experimental Study on Flexural Behavior of Post-tensioning Bonded Partially Prestressed Ultra-high Strength Concrete Beams." *Journal of Harbin Institute of Technology*. 22(2):94–102.

Li, F. M., and Y. S. Yan. 2010. "Experimental Study on Bending Property of Prestressed Concrete Beams with Corroded Steel Strands." *Journal of Building Structures*. 31(2):78–84.

Limongelli, M.G.Siegert, D.Merliot, E.Waeytens, J. Bourquin, F.Vidal, R.Corvec, V.L.Gueguen, L., and L.M. Cottineau (2016). "Damage Detection in a Post Tensioned Concrete Beam- Experimental Investigation." *Engineering Structures*. 128:15–25.

Meng, G., J. Q. Jia, and J. Z. Wang. 2013. "Study on Flexural Behavior of Prestressed Ultra-high Strength Concrete Beams." *Journal of Harbin Engineering University*. 34 (5):575–580.

Minh, H., H. Mutsuyoshi, and K. Niitani. 2007. "Influence of Grouting Condition on Crack and Load-carrying Capacity of Post-tensioned Concrete Beam Due to Chloride-induced Corrosion." *Construction and Building Materials*. 21(7):1568–1575.

Mu, L. J. 2017. *Study on Constructive Model Related Strain Rate of Typical Polymer Materials*. Nanjinjing: Southeast University.

Oh, B. H., and K. S. Kim. 2004. "Shear Behavior of Full-scale Post-tensioned Prestressed Concrete Bridge Girders." *Aci Structural Journal*. 101(2):176–182.

Wang, T. W. 2013. *Structural Test of Civil Engineering*. Wuhan University of Technology Press. Wuhan: In Chinese.

Wang, W. D., and L. H. Han. 2008. "Research on Practical Resilience Model of Load versus Displacement for Concrete Filled Steel Tubular Frame." *Engineering Mechanics*. 25(11):62–69.

Woodward, R. J. 1981. *Conditions within Ducts in Post-tensioned Prestressed Concrete Bridges*. Wokingham, Berkshire United Kingdom: Publication of Transport & Road Research Laboratory.

Xiong, H. X., Z. Yu, and Y. T. Zhang. 2010. "Elastic Modulus of Prestresseg Concrete Beam Based on Damage Mechanics." *Engineering Mechanics*. 27(s2):217–220.

Yao, D. L., J. Q. Jia, and F. Yu. 2013. "Analysis on Shear Ductility of Prestressed Ultra-high Reinforced Concrete Beams." *Journal of Harbin Engineering University*. 34 (5):593–598.

Zhang, Y. T., J. Zhang, and L. Yang. 2017. "Research on the Effects of Prestressing Ratio on the Seismic Capacity of Prestressed Concrete Frame Structures." *Engineering Mechanics*. 34(2):129–136.

Zhao, Z. G. (2012), "Application Researches on Construction Technology of Post-tensioned Pre-stressed Concrete Bridge." [Master dissertation], Northeast Petroleum University.

Zhou, J. M., X. H. Pan, and F. Zhang. 2013. "Experimental Study on Seismic Performance of Post-tensioned Prestressed Concrete Beams Reinforced with 500MPa Rebars." *China Civil Engineering Journal*. 46(5):39–49.

Zhou, Q., and X. C. Zhang. 2015. "Static Load Test and Numberical Analysis of Post-tensioning Pre-stressed Concerte Bridge." *Journal of Wuhan University of Technology*. 37(2):112–115.